Available online at www.sciencedirect.com
SCIENCE DIRECT®
Deep-Sea Research I 51 (2004) 637–652
DEEP-SEA RESEARCH PART I
www.elsevier.com/locate/dsr

Bandwidth similarity at inertial and tidal frequencies in kinetic energy spectra from the Bay of Biscay

Hans van Haren

Department of Physical Oceanography, Royal Netherlands Institute for Sea Research (NIOZ), P.O. Box 59, 1790 AB Den Burg, The Netherlands

Received 11 March 2003; received in revised form 23 September 2003; accepted 26 January 2004

Abstract

Two contrasting mechanical sources may generate internal gravity waves in the ocean: spectrally sharp and spatially localized tide-topography forcing, and widespread and spectrally broad atmospheric forcing. However, their responses were observed very similar in yearlong current observations down the continental slope into the abyssal plain of the Bay of Biscay. This similar response (around semidiurnal tidal and local inertial frequency, respectively) was neither spectrally sharp-like purely deterministic barotropic tidal forcing nor broad-like atmospheric forcing. Instead, it had a limited spectral bandwidth $\Delta\sigma = (0.09 \pm 0.02)\sigma, \sigma$ denoting frequency, which determined 'intermittency'. This similar relative bandwidth in frequency was attributed to ocean response being less dependent on external forcing and primarily dependent on variations in internal wave background conditions, such as stratification, shear, effective inertial frequency, and non-linear interaction. The same relative bandwidth was also found around super-tidal frequencies within the internal wave band associated with inertial–tidal and higher tidal harmonics, because of (i) the above narrow-band character of near-inertial motions in which the initial response to atmospheric disturbances was 'focused', and (ii) the redistribution of inertial and tidal energy to other frequencies through non-linear interactions.

Keywords: Internal waves; Intermittency; Non-linear processes; Bay of Biscay; 46°N; 06°W.

1. Introduction

A stratified ocean can support free 'internal' gravity waves within the frequency (σ) band $f < \sigma < N = (-g\mathrm{d}(\ln\rho)/\mathrm{d}z)^{0.5}$, $N \gg f$, where g denotes the acceleration of gravity, ρ density and f and N the inertial and buoyancy frequency, respectively. Such waves are forced mechanically by the atmosphere (mainly through the generation of inertial motions) or by the conversion of external ('surface') tides through interaction with sloping bottom topography. In this paper, the relative importance and the character of the ocean's response to both types of forcing is examined. The study focuses on the response in the deep ocean, in the vicinity of rough topography of the continental slope in the Bay of Biscay. There, the character of the response seems quite similar, despite the entirely different forcing.

Surface tidal forcing is an extremely narrow-band 'deterministic' phenomenon. It is characterized by the spring-neap cycle modulation, a

E-mail address: hansvh@nioz.nl (H. van Haren).

0967-0637/$ - see front matter © 2004 Elsevier Ltd. All rights reserved.
doi:10.1016/j.dsr.2004.01.006

superposition of predominantly semidiurnal moon (M_2) and sun (S_2) tides. However, this characteristic is generally not found in its response in the ocean interior (for example, Ozmidov, 1965; Magaard and McKee, 1973; Wunsch, 1975; Schott, 1977), with exceptions suggested for (continental) sloping topography (Siedler and Paul, 1991). This general ocean response seems to have a finite bandwidth of $\sim 0.1\,\sigma_{M_2}$, as is inferred from the 'intermittent character' of internal tides (discussion in Ekman, 1931), having a modulation period of ~ 5 days.

Atmospheric (wind stress and pressure) forcing is a broadband signal with energy spread across the entire ocean spectral frequency range, and occurring randomly (intermittently) in time. In the upper O(100 m) of the ocean a transient response of inertial motions is generated after passage of an (atmospheric) disturbance (Pollard and Millard, 1970; Gill, 1982). This response is confined to a relatively narrow band near f, which is communicated into the ocean interior (D'Asaro and Perkins, 1984; Kundu, 1993; Garrett, 2001). Observations discussed by Fu (1981) suggest a bandwidth of $(0.1 \pm 0.05)f$ above rough topography, although the spreading is large (and a universal near-inertial band is not defined). Several suggestions are given for the spectral width of this response. Firstly, the latitudinal (φ) dependence of $f = 2\Omega \sin\varphi$, twice the local vertical component of the Earth's rotation vector Ω, results in a natural (global) enhancement of energy across a finite bandwidth near the inertial frequency due to the curvature of the earth. This is due to interference of incoming and reflected waves at their 'turning latitude', mathematically described by airy functions (Munk and Phillips, 1968). As shown by Munk (1980) and Fu (1981) this 'global' model results in a relatively wide near-inertial band, wider than observed above rough topography (Fu, 1981). Secondly, a smaller finite width of a near-inertial band results from a 'local' generation model due to the finite meridional extent of the forcing (Fu, 1981). Depending on the definition of bandwidth and spatial extent of the forcing, this model gives a near-inertial bandwidth of $\sim 0.1f$ at mid-latitudes. Thirdly, Stewartson and Walton (1976), Fu (1981) and Kunze (1985) associate a finite near-inertial band with variations in background stratification and sub-inertial vorticity.

Here we examine yearlong observations from a moored array of instruments to learn more about the apparent similarity in (relative) bandwidths of so dominant, yet completely differently forced near-inertial and tidal internal motions in the ocean. We define a bandwidth-dependent intermittency factor

$$f_{\mathrm{i}}(\sigma) = \frac{\sigma}{\Delta\sigma}, \tag{1}$$

$$\text{bandwidth } \Delta\sigma = \sigma_{\mathrm{h}} - \sigma_l,$$
$$P(\sigma_l) = P(\sigma_{\mathrm{h}}) = 0.1P(\sigma), \quad \sigma_l < \sigma < \sigma_{\mathrm{h}},$$

where $P(\sigma)$ denotes the spectral (kinetic) energy density and subscripts l and h denote the frequencies lower and higher than σ, respectively. The definition of bandwidth in (1) is stricter than applied by Fu (1981), who uses half- instead of one-tenth-power thresholds. As will be shown, this difference in definition of bandwidth does not so much affect σ_{l} for the near-inertial band, but it does affect σ_{h}, because of the strong asymmetry of the observed (and modeled) bands. For example, the global model of the near-inertial band mentioned above does not pass threshold (1), as it extends only 0.7 decade above the internal wave continuum for mid-latitudes (Munk, 1980; Fu, 1981). When the 0.1 threshold is raised to 0.2, the bandwidth of such 'global' near-inertial peak is $\sim 0.3f$.

The intermittency factor (1) is inversely proportional to the bandwidth parameter defined for surface waves by Longuet-Higgins (1984). Multiplied by period $T(\sigma) = 2\pi/\sigma$, $f_{\mathrm{i}}T$ estimates an average length in time of intermittent occurrence (Fu, 1981), or a wave group passing an instrument. This associates with previous suggestions by Levine (1991) and Thorpe (1999) to study internal wave groups or internal wave intermittency rather than individual internal waves. Associated with (internal) wave groups are possibly strong non-linear interactions and occasional wave breaking (Thorpe, 1999). Following evidence that inertial–tidal interactions dominate super-tidal internal waves (Mihaly et al., 1998; van Haren et al., 1999; van Haren et al., 2002), we also

investigate the widths of bands at these interaction frequencies.

2. Data and methods

2.1. Site and instrumentation

Kinetic energy spectra were analyzed using 11 months of current meter data from eight moorings down the continental slope into the abyssal plain of the Bay of Biscay (Fig. 1). Details were studied using data from the deepest mooring (water depth $H = 4810$ m) at about 100 km from the foot of the steep continental slope, where the bottom slope averaged 0.1° to its nearest neighbor, 50 km in the direction of the continental slope. For reference, results from the Bay of Biscay were compared with data from the abyssal Canary Basin in the eastern Atlantic Ocean ($\sim$20–30°N, 20°W, $H \approx 5000$ m; Siedler and Paul, 1991).

In the Bay of Biscay moorings consisted of 3–4 NBA and Aanderaa current meters between 50 and 1000 m above the bottom below a single buoyancy package. The shallowest mooring consisted of two current meters below an upward looking 75 kHz acoustic Doppler current profiler (ADCP) in a buoyancy collar. Here, we only consider 13 records (Table 1) containing good data

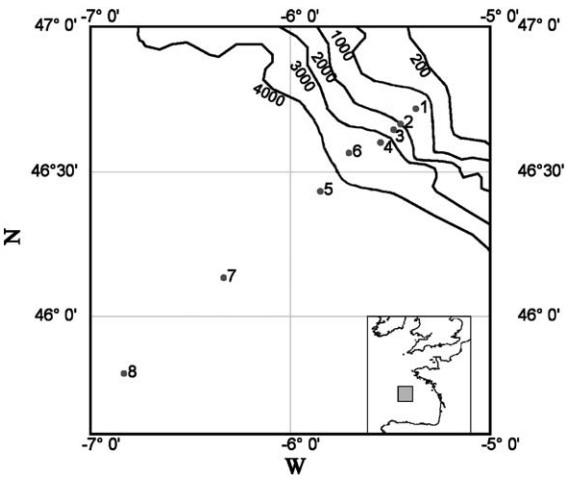

Fig. 1. Mooring positions 1–8 (henceforth named BB1–8) in the Bay of Biscay.

over the entire period of 11 months from positions well outside the bottom boundary layer. Such data were from Aanderaa RCM-8 current meters, sampling at once per 20 min.

Yearlong average baroclinic kinetic energy spectra from the abyssal Bay of Biscay were dominated near the local inertial ("f"; henceforth, a frequency between double quotes denotes a band, not a specific frequency) and semidiurnal tidal frequencies ("D_2"; D for unspecified diurnal tidal as in Pugh, 1987) (Fig. 2). Higher up the continental slope the semidiurnal tidal motions increased in magnitude, being nearer to the suggested source of internal tidal generation near the shelf edge (Pingree and New, 1991). Also higher up the continental slope stratification increased and, correspondingly, the general internal wave band baroclinic kinetic energy, *except* at f and non-linear interaction frequencies involving "f" and "D_2".

2.2. Separating barotropic and baroclinic currents

In unsmoothed spectral detail M_2, S_2 and N_2 were distinguished as deterministic signals by their spiked, narrow-band appearance in the original record (Fig. 3). These signals did not represent small-scale baroclinic, free internal wave motions. This was evidenced by the difference record from two current meters separated by 400 m vertically, showing that tidal spikes were gone. By definition, such difference record did not contain barotropic (often termed 'mode-0') motions or 11 months' coherent large-scale quasi-baroclinic ('mode-1') motions. Barotropic tidal amplitudes and phases were assumed to vary on the extreme long-term only, like variations in topography and the earth-lunar and -solar systems, for example. In yearlong records, they appeared as purely deterministic signals, filling very narrow bands (spikes) in spectra. Coherent baroclinic tidal amplitudes and phases were assumed to vary on climatic decade time scales of varying (large-scale) stratification near an internal tide source like the shelf break (van Haren, 2004). As the focus here is on small-scale internal waves and thus on small-scale internal tidal motions, the above large-scale motions were separated from the rest of the

Table 1
Aanderaa RCM-8 current meter records of 330 days good data return outside the bottom boundary layer in the Bay of Biscay

Mooring	Latitude	Longitude	Water depth (m)	Instrument height above bottom (m)
BB2	46°40′N	005°27′W	2099	500
BB3	46°39′N	005°29′W	2677	1000
BB6	46°34′N	005°42′W	3712	300, 600, 1000
BB5	46°26′N	005°51′W	4322	300, 1000
BB7	46°08′N	006°20′W	4714	300, 600, 1000
BB8	45°48′N	006°50′W	4810	300, 600, 1000

Instruments were moored between July 1995 and June 1996.

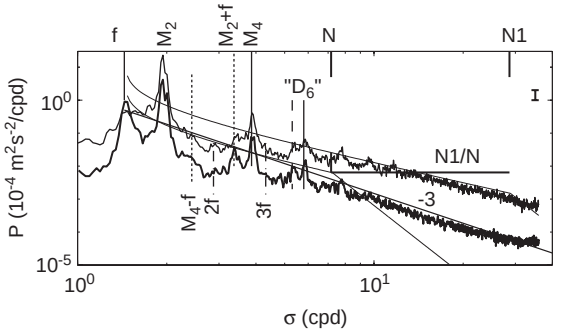

Fig. 2. Moderately smoothed ($\nu \approx 35$ df, degrees of freedom) kinetic energy spectral overview of the internal wave band from observations in the Bay of Biscay at 1000 m above the bottom at moorings BB3, $H = 2677$ m depth (thin, upper spectrum), and BB8, $H = 4810$ m depth (thick, lower). The smooth thin curves represent the model by Garrett and Munk (1972; GM), which are relatively offset by the ratio of the local buoyancy frequencies $N1$ and N, respectively. According to van Haren et al. (2002) energy at inertial-tidal interaction frequencies fall-off with frequency at a rate of σ^{-3}.

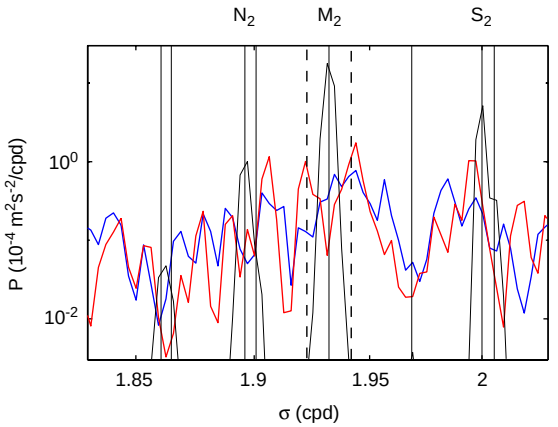

Fig. 3. Semidiurnal tidal band of nearly unsmoothed ($\nu \approx 3$ df) kinetic energy spectra from 11 months of current observations $\boldsymbol{u}$ at $z = -3810$ m, mooring BB8 in the Bay of Biscay. The black spectrum represents the large-scale barotropic part $\boldsymbol{u}_0$. The red spectrum represents the incoherent baroclinic part $\boldsymbol{u}'$, $\boldsymbol{v}'$. For reference, the blue spectrum represents the vertical difference $u(z = -3810\,\text{m}) - u(z = -4210\,\text{m})$, similar for the v-component). Thin vertical solid lines indicate tidal constituents from left to right: $2N_2$, μ_2, N_2, ν_2, M_2, L_2, S_2, K_2. Dashed lines indicate $0.995M_2$ and $1.005M_2$.

internal (tidal) wave band ('(incoherent) baroclinic' motions), which varied with stratification on relatively short sub-inertial time scales.

The split of original currents (u, v) in each record was achieved using sharp band-pass filters, harmonic analysis (Dronkers, 1964). Large-scale ('barotropic' and 'coherent baroclinic') semidiurnal tidal currents (u_0, v_0) were defined by applying such filter using eight semidiurnal harmonic constituent frequencies,

$$u_0 = \sum_n U_n \cos(\varphi_n + \sigma_n t),$$

$$\sigma_n = 2N_2,\ \mu_2, N_2,\ \nu_2,\ M_2,\ L_2,\ S_2,\ K_2$$

$$(1.83 < \sigma_n < 2.03\ \text{cpd}) \qquad (2)$$

for amplitudes U_n and phases φ_n at each depth, similar for v. Frequency was given in cycles per day ($1\ \text{cpd} = 2\pi/86\,400\ \text{s}^{-1}$). Kinetic energy levels in spectra of the rest $(u', v') = (u, v) - (u_0, v_0)$, henceforth 'baroclinic currents', were about equal to those of vertical difference spectra (Fig. 3), implying relatively short vertical scales as anticipated. They were also about equal to the kinetic energy levels of deterministic N_2, ~one decade below those of deterministic M_2 at the deepest mooring above the abyssal plain.

2.3. Spectral analysis: smoothing

In the spectral analysis performed here variable smoothing was applied, $\nu \approx 3-70$ degrees of freedom (df). To examine spectral details, only a single cosine-bell-shaped taper window was used over the entire length of the time series without further smoothing ($\nu \approx 3$ df). Such smoothing resulted in an effective fundamental bandwidth $\delta\sigma_e \approx 2.2\delta\sigma_{fbw}$ (Fig. 4), with $\delta\sigma_{fbw}$ denoting the resolved fundamental bandwidth ($\delta\sigma_{fbw} \approx 0.003$ cpd for an 11 months record). Such nearly raw spectra were used considering some (e.g. tidal) motions deterministic rather than a particular realization of a stochastic process (cf. Fig. 3). Previously, nearly raw spectra were commonly used in studies on surface tides and their non-linear higher harmonics (e.g. Rossiter and Lennon, 1968; Pugh, 1987). Less commonly, they were used in studies on tidal harmonic currents, although governed by similar non-linear processes (Pingree and Maddock, 1978). Statistics usually applied (Jenkins and Watts, 1968) were not considered appropriate for such deterministic signals, and therefore error bars were not indicated in such spectra.

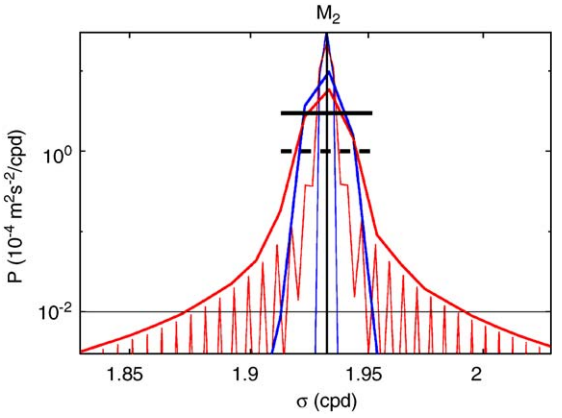

Fig. 4. Effective bandwidths in relation to spectral smoothing of artificial timeseries having identical number of datapoints and sampling frequency as the Bay of Biscay data, but only a single harmonic (M_2) frequency. The figure window is identical to Fig. 3. The thin blue spectral spike is for $\nu \approx 3$ df, whilst the thick blue spectrum is for $\nu \approx 8$ df. The bandwidth limits are inferred from the intersection of the spectra with the solid and dashed black lines, respectively, at one decade below the peak values. At $\nu \approx 3$ df spectra have a frequency resolution of ~ 0.006 cpd. In red are spectra with the same variation in smoothing for a time series of non-zero data at half the number of points and zero otherwise. This reduces the peak values, but also broadens the spectral width, due to the abrupt transition from non-zero to zero data values.

Uncertainty existed about the stochastic character of motions at frequencies other than tidal constituent frequencies. For such motions heavier smoothing was achieved by applying the same taper window over half-overlapping sub-sections of the time series. This resulted in a broadening of the effective fundamental bandwidth (Fig. 4). In the present study on internal tidal and inertial wave motions an optimum between maximal frequency resolution and reliable statistics was found by weak-moderate smoothing ($\nu \approx 8$ df), so that the error bounds were less than the 0.1 decade energy criterion (1) for determining the bandwidth. For comparison, Fu (1981) applied spectral smoothing using at least $\nu > 14$ df, so that his frequency resolution was ± 0.024f. Note that the smoothing chosen here did not introduce artificial spectral ripples, inferred from the comparison of the observed energy at non-tidal constituent frequencies (Fig. 3) and frequency response functions of artificial signals (Fig. 4). Also note that in the present paper all (details of) spectra are plotted in log–log fashion, so that (relative) bandwidths can be compared directly within the same figure using a ruler.

2.4. Bandwidth computation

In practice, the extraction of distinguished frequency bands from baroclinic records including relatively large energy at unknown frequencies required some additional criteria to definition (1). The first step in determining a bandwidth was by smoothing the spectrum such that the 95% statistical significance levels $P(\sigma) \pm \chi_{95}(\sigma)$ were less than a decade apart in energy, so that the band limits according to (1), $P(\sigma_l) = P(\sigma_h) = 0.1P(\sigma)$, were statistically separated from the peak value

$$P(\sigma_l) + \chi_{95}(\sigma_l) < P(\sigma) - \chi_{95}(\sigma)$$

similar for σ_h. The smoothing should result in an effective fundamental bandwidth $\delta\sigma_e \ll 0.1$ cpd.

Here, typically $\delta\sigma_e \approx 0.015$ cpd is used. Secondly, the frequency of the maximum peak energy was sought within a frequency range of

$$\sigma_0 - 0.2 < \sigma < \sigma_0 + 0.2 \text{ cpd}, \ \sigma_0 = f \text{ or } M_2. \quad (3)$$

Thirdly, two searches for bandwidth limits were performed; one from the peak value to lower and higher frequencies until meeting criterion (1) within bounds (3); another from the low and high frequencies bounds in (3) towards the peak frequency searching for the levels at least exceeding twice the mean energy level at frequencies outside band (3) and until meeting criterion (1). In case for closely spaced inertial and semidiurnal bands as at mid-latitudes a single mean background continuum level was calculated from $1.6 < \sigma < 1.7$ cpd (Fig. 5). Fourthly, all the above criteria should be passed by a consecutive frequency range having a width of at least one effective fundamental band, so that for example a spectral dip $< 0.1P(\sigma)$ at just a single frequency did not set a bandwidth boundary (σ_l or σ_h) at that particular frequency. Results from the two searches were averaged, excluding bandwidth estimates that did not pass the criteria to (1), as

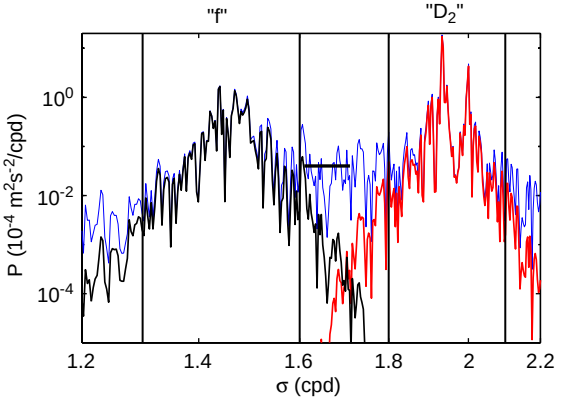

Fig. 5. Inertial and semidiurnal tidal band of nearly unsmoothed ($\nu \approx 3$ df) kinetic energy spectra from 11 months of current observations $\boldsymbol{u}$ at $z = -3810$ m, mooring BB8 in the Bay of Biscay. The blue spectrum represents the spectrum for original current data. The black and red spectra are after band-pass filtering, with half-power filter cut-offs at the solid vertical lines. The horizontal vertical line indicates the level of continuum energy between $1.61 < \sigma < 1.71$ cpd, used as reference for finding bandwidth limits.

at some locations for inertial motions. The results for the two searches did not differ by more than 20% and their differences largely determined the standard deviations around the mean results.

2.5. Band-pass filters

In order to compare the contents of different frequency bands in the time domain original time series were band-pass filtered (Fig. 5). The inertial band was filtered using half-power cut-off frequencies at $\sigma = 1.3$, 1.6 cpd, or a pass-band of $\sim 0.2f$. The semidiurnal tidal band filter passed signals between $1.8 < \sigma < 2.1$ cpd. The band "$M_2 + f$" was filtered between $3.1 < \sigma < 3.6$ cpd and "D_4" between $3.6 < \sigma < 4.1$ cpd, resulting in a pass-band of $\sim 0.13M_4$. The modified Kaiser–Bessel-cosine symmetric filters (Parks and Burrus, 1987) were trimmed for proper pass- and stop-band characteristics (Fig. 5).

2.6. Waves?

In single current meter records, the relative importance of free internal waves with respect to other motions like turbulent eddies can be estimated by investigating rotary spectra. The kinetic energy spectrum is decomposed into two rotary spectra describing counterrotating circular motions (Gonella, 1972):

$$P_{KE}(\sigma) = P_{-}(\sigma) + P_{+}(\sigma) \quad (4)$$

with $P_{-}(\sigma)$ the clockwise spectrum and $P_{+}(\sigma)$ the anti-clockwise spectrum. Gonella (1972) introduced several useful spectral properties including 'rotary coefficient':

$$C_R(\sigma) = (P_{-}(\sigma) - P_{+}(\sigma))/P_{KE}(\sigma), \quad (5)$$

denoting the polarization of the horizontal current ellipses. C_R is equal to zero for purely rectilinear motion and equal to ± 1 for purely circular motion. Under symmetric (linear or non-linear) dynamics and neglecting frictional stresses

$$C_R(\sigma) = \frac{2\sigma f}{\sigma^2 + f^2}. \quad (6)$$

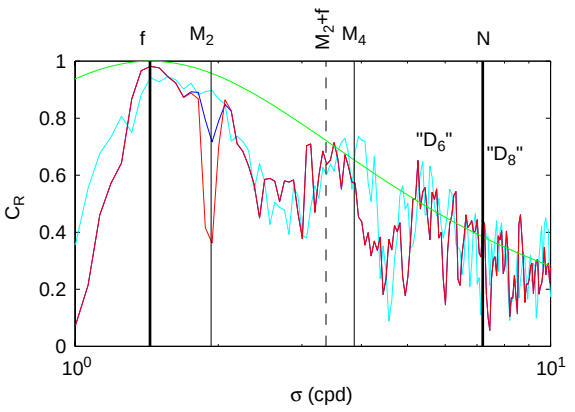

Fig. 6. Rotary coefficient (5) from smoothed ($\nu \approx 70$ df) rotary spectra from 11 months of current observations at 1000 m above the bottom in the Bay of Biscay. The red spectrum represents original current data $\boldsymbol{u}$ from mooring BB8, and the nearly similar dark-blue spectrum is for the baroclinic part $\boldsymbol{u}'$. The light-blue spectrum represents original current data from mooring BB3. The green curve is the free wave model (6).

Using the same observations from the Bay of Biscay, van Haren (2003) found that they collapsed to free wave theory (6) at inertial and non-linear inertial–tidal interaction frequencies like M_2+f, M_4 (Fig. 6). It was also found that energy (and polarization) were much larger (clockwise) at M_2+f than (anti-clockwise) at M_2-f, the associated non-linear component outside the internal wave band. This confirmed observations by Alford (2001), but contrasted with a kinematic model by the same author describing equal amplitudes of (opposing) rotary components of observed $K_1 \pm f$. Alford (2001) and van Haren (2003) concluded that motions at M_2+f were likely free internal waves, although possibly locally generated through non-linear advection.

As for semidiurnal tidal motions in Fig. 6, note their near-rectilinear character above the abyssal plain, evidence of dominant barotropic tidal motions. More internal tidal wave-like near-circular polarization was observed for baroclinic motions at that site and for coherent-baroclinic motions half-way the continental slope, closer to the assumed internal tidal wave source at the shelf break (Pingree and New, 1991).

3. Observations

3.1. General observations of baroclinic current spectra

A first glance at yearlong spectra from the Bay of Biscay (Fig. 2) suggested that the energy of the ocean response at frequencies f and M_2 ($\sigma_{M_2}/\sigma_f \approx 1.33$) was restricted to recognizable bands of indeed roughly similar width. This confirmed suggestions from literature cited in the Introduction, in contrast with the spectra of their forcing mechanisms. The energy at the enhanced bands decreased faster with frequency than spectral fall-off rate of the canonical internal wave continuum: $P(\sigma) \sim N\sigma^{-2}$ (Garrett and Munk, 1972; GM).

3.2. Details of "f" and "D_2"

In the nearly raw baroclinic kinetic energy spectrum above the abyssal plain in the Bay of Biscay (Fig. 7), we observed a central frequency at $1.023f$ and peaks at $1.002f$ and $1.035f$, to within our resolution of 0.002f. This central frequency was close to values observed by Fu (1981) for rough topography in the deep ocean and by D'Asaro and Perkins (1984). It was also close to the value of $1.03f$ (for $z = -4000$ m) predicted by Garrett (2001) using theoretical considerations for predominantly downward and equatorward propagating near-inertial energy generated near the surface.

The baroclinic semidiurnal tidal band had similar shape as the baroclinic f-band, but mirror-imaged and having its steepest side at the high-frequency side. "D_2" was centered at $1.005M_2$, showing also four major peaks like in "f". Although a relatively large gap existed between peaks near (not at) M_2 and S_2, enhanced energy at semidiurnal frequencies was part of a wider band encompassing the major semidiurnal tidal constituents: the smoothed spectrum in Fig. 7. Also in that smoothed version of the spectrum the near-inertial and semidiurnal tidal bands were comparable. The energy at frequencies like $1.005M_2$ and $1.023f$ was comparable to that of known tidal constituent barotropic N_2.

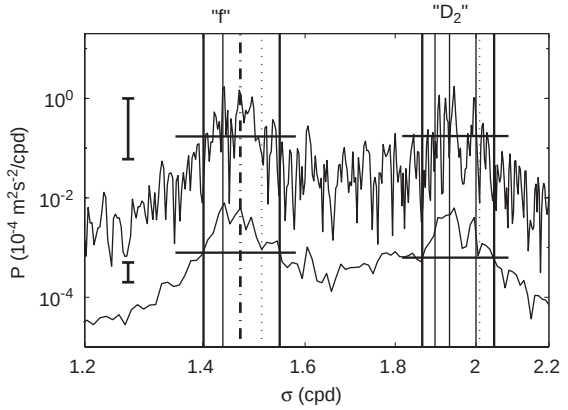

Fig. 7. Kinetic energy spectral bandwidths of inertial and baroclinic semidiurnal tidal currents at $z=-3810$ m, mooring BB8 in the Bay of Biscay. The bandwidths (between heavy solid vertical lines) are determined according to (1) and Section 2.4: (0.975, 1.077)f and (0.965, 1.06)M_2. The bandwidths are shown with unsmoothed ($\nu \approx 3$ df; heavy upper line) and weakly smoothed ($\nu \approx 8$ df; thin line, arbitrarily offset vertically) spectra from 11 months of $\boldsymbol{u}'$. Thin vertical solid lines indicate from left to right the frequencies f, N_2, M_2 and S_2. The thick dashed line indicates 1.023f. The dotted lines indicate 'gaps' at 1.052f and 1.04M_2, also typical for each band and causing relatively large errors in mean relative bandwidth (7). Thick horizontal lines indicate energy levels one decade below the maximum energy within each band.

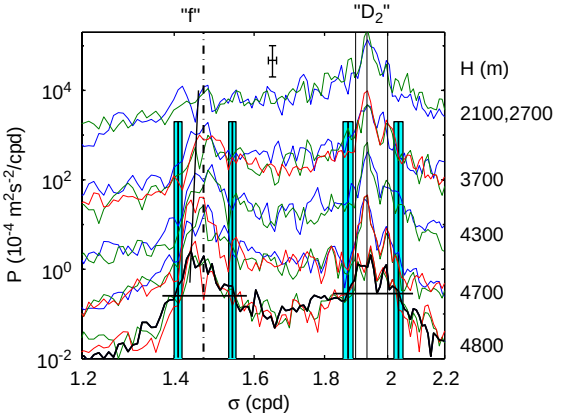

Fig. 8. Inertial and semidiurnal tidal band of weakly smoothed ($\nu \approx 8$ df) kinetic energy spectra from all records of 11 months of $\boldsymbol{u}'$ outside the bottom boundary layer in the Bay of Biscay (cf. Table 1). The vertical filled blue bars indicate the mean and 1 std of all bandwidth estimates, excluding the upper two spectra for the inertial bandwidth. Spectra are offset vertically for each mooring. The single records for moorings BB2 and BB3 are grouped together. The heavy black spectrum is the thin spectrum in Fig. 7. The 95% level of statistical significance is given in the central upper part, together with the effective bandwidth. The heavy dash–dotted line indicates 1.023f (at latitude of mooring BB8). The solid line slightly slanted towards the vertical represents all local inertial frequencies when crossing the level of peak values within the near-inertial bands. Within "D_2" N_2, M_2 and S_2 are indicated by thin vertical lines.

From the abyssal plain up the continental slope the ratio of inertial over tidal baroclinic energy decreased (Fig. 8). However, the relative *width* of both "f" and "D_2" remained closely similar, so that, using the method described in (1) and Section 2.4, the average relative bandwidth over the two bands over all 13 current meter records was

$$\Delta\sigma/\sigma = 0.09 \pm 0.02.$$

and intermittency factor (1) was more or less constant and the bandwidth depended linearly on frequency. Specified per frequency band it was found for tides only: $\Delta\sigma/\sigma_{D2} = 0.086 \pm 0.016$; for inertial motions: $\Delta\sigma/\sigma_f = 0.090 \pm 0.013$, excluding undetermined data from mooring 2. The relatively large error (1 std) was mainly due to the spectral environment from which the two bands emerged in relation to the (arbitrary) criteria used. No systematic variation of relative bandwidth outside the given error bars was detected under different conditions over the continental slope (Fig. 8).

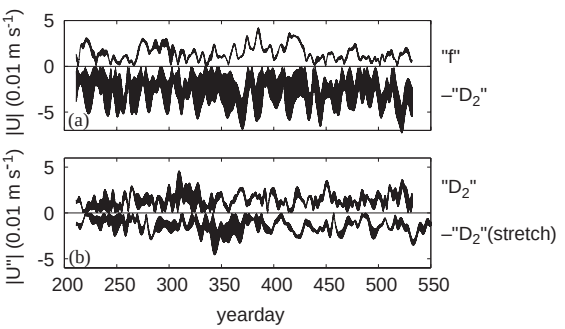

Fig. 9. Time series of amplitudes of band-pass filtered currents (indicated by $\langle\,\rangle$). (a) Near-inertial and (negative amplitude of) semidiurnal tidal bands $|<\boldsymbol{u}>|$ of original data at $z=-3810$ m, mooring BB8 in the Bay of Biscay. (b) Semidiurnal band of baroclinic $|<\boldsymbol{u}'>|$. The (negative amplitude of the) latter is also shown in stretched time coordinates (see text).

The spectral similarity between baroclinic "f" and "D_2" was also observed in the time domain after application of band pass filters (Fig. 9). In

otherwise unprocessed original data modulations of amplitude variance from these bands were quite different (Fig. 9a). Clearly, a spring–neap cycle was distinguished for the tidal band but not for the inertial band. Also different between the graphs of amplitudes was the line thickness, reflecting the modulation with time of ellipse polarization within a band and generally appearing thin for "f" and thick for "D_2". Lines appeared thick when ellipticity of the horizontal motions within a frequency band was small, typical for large-scale near-rectilinear tidal currents above the abyssal plain. Lines appeared thin for near-circular motions. As expected from the rotary spectra (Fig. 6), the line thickness of baroclinic "D_2" (Fig. 9b) appeared much thinner than the line thickness of the original "D_2" (Fig. 9a), implying that baroclinic motions were more circularly polarized, as expected for internal wave motions. The variation with time of line thickness, or the modulation of polarization, reflected the (dominance of) internal wave character within a band. Note also that the modulation of the amplitude of baroclinic "D_2", reflected by the number of peaks in a line, was faster than the spring–neap cycle, having $\sim$6 days period.

A 'fast' modulation was suggested from (7) for *both* baroclinic bands (because the inertial and tidal frequencies are not very far apart at mid-latitudes). In Fig. 9a, 48 peaks were distinguished for "f", so that $f_i T_f = 330/(48 \pm 1) = 6.9 \pm 0.15$ days $= (11.2 \pm 0.2) T_f$, T_f the inertial period. In Fig. 9b, 60 peaks were distinguished for "D_2", so that $f_i T_{D2} = 330/(60 \pm 1) = 5.5 \pm 0.15$ days $= (10.6 \pm 0.2) T_{D2}$, T_{D2} the tidal period. The similarity between the inertial and the semidiurnal tidal band signal was inferred after stretching the time axis of the baroclinic "D_2" time series by a factor of $T_f/T_{M2} \approx 1.33$ (Fig. 9b). The number of amplitude peaks in the stretched "D_2" record was nearly the same over the same period of time as for "f". The O(1 week) fast modulation was weakly modulated on a (slow) 50–100 days time scale, showing about five periods of enhanced baroclinic "D_2" variance (being enhanced over a period of $\pm$10 days around days 260, 310, 370, 440 and 510). The "f" more clearly showed a slow modulation of roughly the same periodicity, but being enhanced at different times ($\pm$10 days around days 220, 280, 380, 415 and 470). Most energy at sub-inertial frequencies was at 0.01–0.02 cpd.

3.3. Details of "M_2+f" and "D_4"

The suggested observation that the shape of the combined "f"+"D_2"-band was copied onto the bands "M_2+f"+"D_4", "M_4+f"+"D_6", "M_6+f"+"D_8" (Fig. 2) was evaluated by examining the fourth-diurnal bands "M_2+f" and "D_4" (Figs. 10 and 11).

The spectral widths of these frequency bands (Fig. 10) seemed also according to (7), although we could not compute them directly since they did not pass the criteria to (1). Their maximum value was only just one decade above the mean level of the direct spectral environment. Just simple summing of the peak frequencies, for example as a result of non-linear advection, of the baroclinic bands "f" and "D_2" using an energy reduction following $\sim\sigma^{-3}$ fall-off rate (Fig. 2) resulted in (enhanced) higher harmonic bands that matched the observed frequency bounds of "M_2+f" and "D_4".

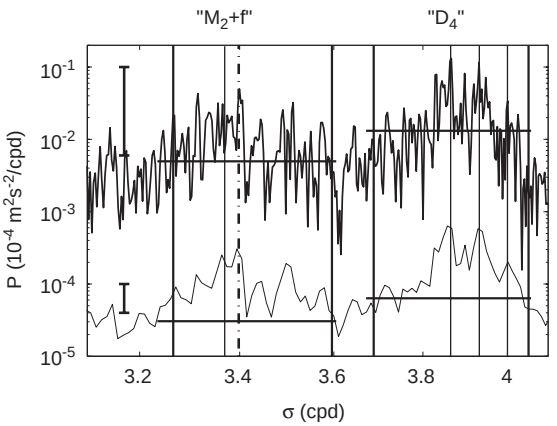

Fig. 10. As Fig. 7, but for fourth-diurnal frequencies including bands "M_2+f" and "D_4". Thin vertical lines indicate from left to right: M_2+f, M_4, MS_4 and S_4. The thick dashed line indicates $M_2+1.023f$. Thick vertical lines indicate bandwidths $(0.975f+0.965M_2,\ 1.077f+1.06M_2)$ and $(0.955,\ 1.05)M_4$, taken from the inertial and semidiurnal tidal bandwidths. These bandwidths are slightly (<10%) smaller and larger, respectively, than when computed from the thin spectrum is this figure using only the criteria given for (1).

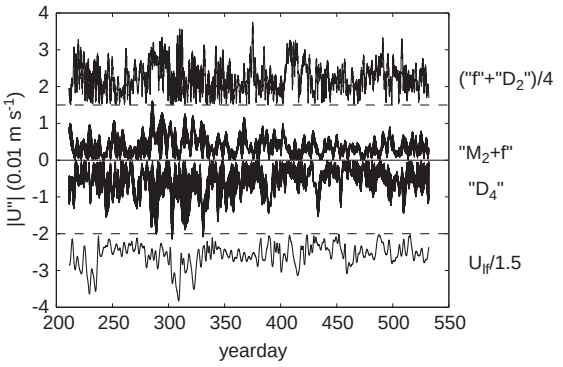

Fig. 11. As Fig. 9 but for fourth-diurnal band-pass filtered time series. They are compared with the combined inertial and baroclinic semidiurnal tidal band-pass filtered series (arbitrarily offset vertically and at a different scale), and with the sub-inertial filtered low-frequency (lf) series negatively offset vertically.

For example, $\sigma_\ell(f)+\sigma_\ell(M_2)\approx\sigma_\ell(M_2+f)$, $\sigma_h(f)+\sigma_h(M_2)\approx\sigma_h(M_2+f)$, and similar for the overtides. The possible mechanisms generating such higher harmonic bands are discussed in Section 4. This suggested preservation of (7), which was confirmed by inspecting individual higher tidal harmonics M_4, MS_4 and S_4, but also from $2\times1.005M_2$ dominating "D_4". Such preservation was also observed in "M_2+f", being centered at $M_2+1.023f$, and in time series of band-pass filtered signals (Fig. 11). The number of variance peaks in Fig. 11 also confirmed (7).

Like data in Fig. 9b, a slow (50–100 days) modulation of the amplitude variance of the two fourth-diurnal bands was observed with enhanced amplitudes during about ±10 days around days 230, 300, 400 and 500 (Fig. 11). The slow modulation of both bands reflected the slow modulation of the sum of "f" and "D_2" (uppermost trace in Fig. 11) and the 400 m difference of the sub-inertial ('low-frequency' $\sigma<0.1$ cpd) signal (lowest trace in Fig. 11). Statistically, no significant coherence was found for these low-frequency modulations. However, such coherence was only expected for strictly local generation, but not for free propagation of waves observed after having traveled through a remote varying background.

3.4. "f" and "D_2" in the Canary Basin

For reference, yearlong observations from IfM-Kiel moorings in the abyssal Canary Basin ($\sigma_{D2}/\sigma_f\geqslant1.9$) were inspected near "$f$" and "$D_2$" (Fig. 12). Because topographic features were far away as moorings were halfway between the Mid-Atlantic Ridge and the African coast, different baroclinic currents were expected than in the Bay of Biscay. However, Canary Basin baroclinic tidal currents showed the same relative bandwidth as in (7), well within 1 std. The relative bandwidth of "f" appeared larger, but only exceeded (7)+1 std when the criteria for computing (1) were not met. When the peak in "f" was sufficiently larger than the immediate spectral environment, as for the

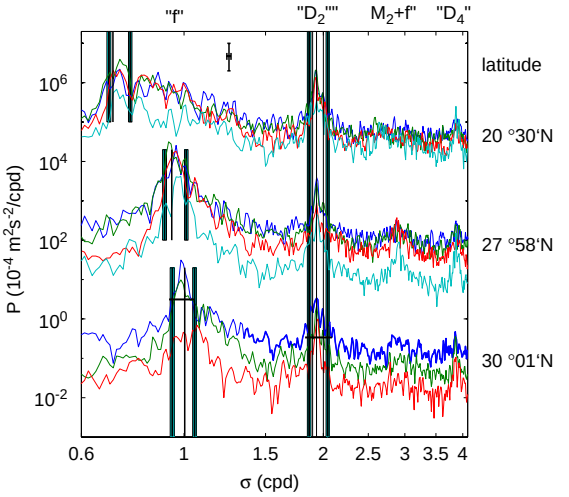

Fig. 12. Similar to Fig. 8, but including the fourth-diurnal bands, for 9 months of 2-hourly observations from the abyssal Canary Basin (along 25°W, $H\approx5000$ m; Siedler and Paul, 1991). Data are from the following depths: at ~30°N 141 m (blue), 1000 m (green), 5175 m (red); at ~28°N 166 m (blue), 261 m (green), 1130 m (red), 5190 m (light blue); at ~21°N 405 m (blue), 610 m (green), 1255 m (red), 4505 m (light blue). The vertical filled blue bars for the semidiurnal tidal band are computed as before with mean $(\Delta\sigma/\sigma)_{D2}=0.09\pm0.017$, about 5% larger than for the Bay of Biscay. Computations for the near-inertial band were more difficult, because less than half the spectra passed the criteria for bandwidth computation and because the peak frequency varied. The mean relative bandwidth for those spectra passing criteria is $(\Delta\sigma/\sigma)_f=0.11\pm0.019$, and this band is indicated for each of the groups of spectra with arbitrary shift of central frequency.

upper two current meter records near 30°N and for the lower two records observed near 28°N, (7) was confirmed to within 1 std. A similar correspondence was found for "M_2+f" and "D_4", when they exceeded internal wave continuum levels. We will not elaborate on an explanation for the strongly reduced peak in "f", especially near 20°N.

4. Discussion

The resemblance in relative frequency bandwidth of the inertial and semidiurnal tidal internal wave bands is observed well within rather large error bounds. As a result, a resemblance in absolute bandwidth cannot be ruled out statistically for the Bay of Biscay data, as it falls just within the 95% significance levels (but outside these levels for the significant Canary Basin data and for the fourth-diurnal bands in the Bay of Biscay). However, in both cases the observed resemblance in (relative or absolute) bandwidth of the inertial and semidiurnal bands and the fourth-diurnal bands suggests a common cause. Because of their completely different sources, the only common cause seems the background supporting the internal gravity waves. Although sophisticated (linear) models with realistic topography and realistic but time-independent $N(z)$ may show a complex beam pattern (e.g. Gerkema, 2002), such modeling will yield unrealistic spectra consisting of monochromatic peaks from records at fixed positions. Below the hypothesis is discussed that (sub-inertial) variations in background conditions dominate the shape of internal wave bands, intermittency, and therefore the measurement of internal waves at a single location. It is further hypothesized that, as a common background variation implies conservation of absolute bandwidth, a more complex non-linear or resonance mechanism is required additionally to preserve relative bandwidth. Following Section 3.2, distinction is made between slow (50–100 days) and fast (1 week) modulations. The above hypothesis somewhat contrasts with many different sources, like small- and large-scale topography variations (St. Laurent and Garrett, 2002) and small- and large-scale atmospheric forcing, yielding possibly different *wavenumber* bandwidths of internal tidal and inertial motions. This also contrasts with global models of near-inertial wave reflection, yielding a (much) broader near-inertial bandwidth than observed, as was noted previously by Fu (1981) for observations above rough topography. It also seems to contrast with local generation of near-inertial motions modeled by Fu (1981), since this requires a particular spatial extent of the source of O(150 km), apparently coincidentally matching that of internal tidal response and varying with latitude to preserve relative bandwidth.

As the present observations cover a limited part of the ocean, only suggestions for possible common causes can be given here. Future modeling should reveal mechanisms behind forcing and redistribution of internal wave energy, when it is dominated at inertial, tidal and their (non-linear) interaction frequencies.

4.1. Does the background determine bandwidth-limited internal wave band spectra?

The common characteristic of all internal gravity waves is the restoring force that depends on N. Any variation in N results in (a) a variation in internal wave energy following GM, (b) a variation of the free wave frequency range, and (c) a change in the direction of propagation of internal wave energy. Above sloping topography internal waves are modeled using ray theory. For a monochromatic wave the directions of rays of enhanced internal wave energy are inclined to the horizontal at an angle $\alpha(\sigma, f_{\mathrm{eff}}(z, t), N(z, t))$ determined by the dispersion relation at a fixed latitude,

$$\sin^2\alpha = \frac{\sigma^2 - f_{\mathrm{eff}}^2}{N^2 - f_{\mathrm{eff}}^2}, \tag{8}$$

where variations in background low-frequency vorticity (ζ) modify the 'effective inertial frequency' $f_{\mathrm{eff}} = f + \zeta/2$ (Mooers, 1975; Kunze, 1985). It is easily verified that 6% variation in $f_{\mathrm{eff}}(z, t)$ or in $N(z, t) \approx \mathrm{O}(10f)$ has the same effect on the ray angle as considering a different neighboring major tidal constituent (M_2 instead of S_2), at

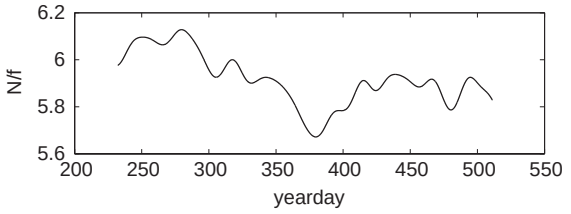

Fig. 13. Low-pass filtered (cut-off at ~ 0.05 cpd) time series of $N == (\alpha g/\rho \Delta T/\Delta z)^{0.5}$ from temperature records from current meters at $z = -3810$ m and -4210 m (BB8), using $\alpha = 0.16$ thermal expansion coefficient (inferred from T–S relationship in CTD observations).

moderate latitudes. Such amount of variation in background conditions is even more dramatic for near-inertial motions: it determines whether they will propagate away as internal waves or not. Locally near the moorings, slow variations of up to 8% were estimated in low-pass filtered, 400 m mean N for the period of moored observations (Fig. 13). For tides, using the (ray) model results by Pingree and New (1991) this amount of N-variation implies an estimated change of 1000 m in a monochromatic semidiurnal tidal ray height at BB8 (150 km, one bottom and one near-surface reflection away from the shelf edge). This height variation is much larger than the estimated beam width of ~ 500 m (Pingree and New, 1991). It is noted that after reflection at a near-surface pycnocline in summer the ray may become very diffuse, according to model results by Gerkema (2001). Further quantitative effects on internal wave bandwidths were not established here, because information on variations in the background conditions along the entire rays of the internal waves from their source is needed. Also, (spatially) different inertial and tidal internal wave sources have not been accounted for. These may cause interference and amplitude and phase modulations at any position away from a source due to waves incoming from different sources. Qualitatively, the above variations in the background conditions not only affect the ray direction but also the registration of internal wave frequency bandwidths, because rays move in- and out-of-reach of the moored instruments (van Haren, 2004). As a result, an instrument moored at a fixed position in space can register finite bandwidth internal waves which are monochromatic in beam coordinates but that are measured varying on the time scale of variation of the background conditions. Slow variations in N and f_{eff} are caused by variations in large-scale currents and shear. However, faster variations, evidence of sudden nonlinear-like variations in N (Fig. 13), can imply an important role for near-inertial motions, as is suggested below.

In contrast with internal tides being forced continuously at a deterministic frequency, near-inertial internal waves experience (fast) amplitude modulation at the source. As near-inertial motions and shear are by nature part of the 'background' for all other internal waves, it is suggested that their fast amplitude modulation can be related to finite bandwidth of all baroclinic motions. Near-inertial shear dominates all internal wave shear and therefore interior diapycnal mixing across enhanced stratification (van Haren et al., 1999) and is also large near an internal tidal wave source (van Aken, unpublished results from the single ADCP at BB1). This is because of the much smaller ($\frac{1}{3}$ or less) vertical length scale for near-inertial motions compared to that of internal tidal motions. The inference is that near-inertial motions set the spatial scales of internal waves. Assuming that near-inertial motions are generated near the surface by atmospheric disturbances of several 100 km horizontal (hence, also meridional) extent typically, we expect $\Delta\sigma \approx \sin(\Delta\varphi)f = (0.03$–$0.10)f$ at mid-latitudes (Fu, 1981). Typical (synoptic) time scale of variation in forcing is 3–5 days, or 5–9 inertial periods, at mid-latitudes. As a result, the disturbance sets the frequency range for enhanced near-inertial energy. Variation in near-inertial energy implies variation in near-inertial shear amplitude, which thus varies on the synoptic timescale and not with the inertial period. This can also be understood because near-inertial motions are circularly polarized, and near-inertial shear too, by definition, so that the amplitude can only vary on the timescale of the modulator. Like other internal waves, propagating near-inertial waves can modify local N by an amount ΔN through straining on the relatively fast synoptic time scales, thereby modulating the amplitude of internal

gravity waves and also allowing generation of internal waves at the natural frequency of oscillation $N+\Delta N$. Once motions near f and N are established they determine the modulation of other internal waves by their spatial and temporal variations. Thus, other (e.g. tidal) internal waves traveling from specific sources through (and interacting with) the same varying background will experience the same variation as near-inertial internal waves. Note that, because of different sources, modulations of the internal tidal wave band need not be registered simultaneously with near-inertial enhancement by a single instrument. The locally non-linearly generated higher-frequency internal waves also contribute to background variations. They (occasionally) cause near-inertial and tidal wave profiles to sharpen as in cnoidal or Stokes waves, thereby enhancing the possibility of wave breaking (van Haren et al., 2002).

Therefore, the observed relative bandwidth of the non-linear fourth-diurnal bands may have two causes. Firstly, the (enhanced) motions may be locally generated through non-linear advection, as is typical for generation of overtides in shelf seas (Pingree and Maddock, 1978). Numerical modeling by Xing and Davies (2002) demonstrated the importance of such non-linear advection between internal waves, which is different from (quasi-)linear advection of internal waves by the (known) barotropic tidal current. Although (quasi-)linear advection may principally result in amplitude increase (just like non-linear advection) following parametric excitation, its spectral result is not commensurate the present observations. As the barotropic tidal current is dominated at a single harmonic constituent (M_2), (quasi-)linear advection would yield a "D_4" bandwidth (absolute) equal to "D_2", but half the *relative* bandwidth (7). This is contrary to the present observations. Secondly, they may be remotely generated, propagating as free waves through (and interacting with) the same (slowly varying) background as near-inertial and tidal internal waves before reaching the instrument sites. Both causes (statistically) yield the same relative bandwidth, provided the spatial (latitudinal) dependence of background variations is not important for the second cause. Apparently, some resonance mechanism is at work. It is suggested that, following variations with time in background conditions, a (weakly) non-linear internal wave train may be subject to sideband instability, as demonstrated for surface waves by Benjamin and Feir (1967). For surface waves, the result is growth of motions in a limited range of frequencies ($\Delta\sigma/\sigma = 2\sqrt{2}\,ka$, a the amplitude and k the wavenumber) at the expense of the source frequency. The key question is why instability growth is limited to result in packets of ~ 10 waves, so that $ka \approx 0.033$, a constant?

4.2. How universal may the observed bandwidth (7) be for water waves?

The observations from the Bay of Biscay and the Canary Basin were from two contrasting sites (with different topography and σ_f/σ_{D2} ratio). The observed similarity in relative bandwidths around inertial, tidal and higher harmonic frequencies was found in quite a few, although not all records. This contrasts with the more varying observations of the near-inertial bandwidth by Fu (1981): 0.05–0.19f for the POLYMODE II area. This contrast may be coincidental. However, it could be due to the larger smoothing applied by Fu, or the difference in definition of the bandwidth. Nevertheless, Fu's mean value 0.097 ± 0.047f for the near-inertial bandwidth at mid-latitudes is close to (7). Roughly similar values have been observed by, for instance, Webster (1968), Pollard and Millard (1970), Kunze (1985). This suggests that wave modulations are triggered by, but further independent of variations with time in background conditions.

Besides several open ocean observations of internal tidal intermittency not associated with spring–neap cycle (Magaard and McKee, 1973; Wunsch, 1975; Schott, 1977; Huthnance and Baines, 1982), intermittency is also found in different areas at different frequencies. Internal tidal intermittency is also reported for shelf seas (van Haren and Maas, 1987), also showing amplitude modulations of 4–7 days periods. Given uncertainties in the separation of the baroclinic signals from the original records and possible errors induced through band-pass filtering

(Wunsch, 1975), (7) seems well confirmed for "D_2". However, it is noted that the observations by van Haren and Maas (1987) are dissonant, as they are not attributed to free internal tidal waves but to tidal advection of varying stratification. Does this imply that a wave character is less important and that any non-linear modification of stratification leads to similar scales of variation? On the other hand, if non-linear interaction between background and internal waves is important, all enhanced frequency bands in the entire internal wave band may appear in limited bands as well, including high-frequency internal waves.

High-frequency internal wave bands have been inspected previously. For example, internal waves near the buoyancy frequency seem to occur in groups of 4–12 waves (Brekhovskikh et al., 1975; Marmorino, 1987; Marmorino et al., 1987), implying a bandwidth of 0.08–0.25N. Such observations are also made for surface waves and Longuet-Higgins (1984) finds his bandwidth parameter varying between $0.05 < 1/f_i < 0.15$ for swell and $0.11 < 1/f_i < 0.24$ for wind waves. Hasselmann et al. (1973) report similar values for JONSWAP spectra (cf. Fig. 14).

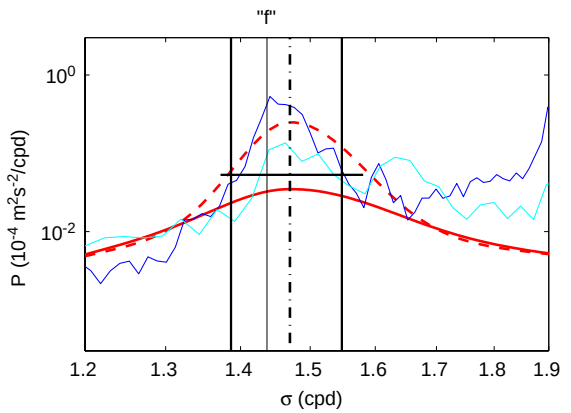

Fig. 14. Comparison between surface wave spectra and observed near-inertial band data as in Figs. 7 and 12, but slightly more smoothed ($\nu \approx 12$ df). The blue spectrum is for $z = -3810$ m from mooring BB8 in the Bay of Biscay, the light-blue spectrum is from $z = -4505$ m at $\sim 21°$N in the Canary Basin shifted in frequency so that local f matches that of BB8. In red are surface wave spectra with their peak frequency scaled to f of BB8. The solid red spectrum is a 'sharp JONSWAP' spectrum (Hasselmann et al., 1973). The dashed red line is an 'unrealistic' (steeper than the steepest) JONSWAP spectrum.

The conservation of bandwidth for (weakly non-linear) surface wave spectra is attributed to a balance of energy input, dissipation and internal redistribution through weak non-linear resonant interactions (Hasselmann et al., 1973). Thorpe (1999) suggests that wave breaking within an internal wave group may just balance dispersion of individual waves, besides its relevance for ocean mixing. Non-linearity may add to redistribution of energy to other internal wave frequencies and to the possibility of breaking within a group. Hence, the suggestion by Levine (1991) and Thorpe (1999) to study (internal) wave groups seems also important for the construction of the entire internal wave band. This supports suggestions by Briscoe (1999) that deep-ocean internal waves are not horizontally isotropic over 75 (and longer) periods. Future work should focus on the mechanism behind the self-similar character of such groups of ~ 10 waves and on the dynamics of internal waves. First however, more observations need to be analyzed to verify (7) in relation with variations in near-inertial peak height and in relation to variations in source, continuing the work by Fu (1981). We also need time series that are (much) longer than 1 year.

5. Conclusions

Eleven months of current meter data were analyzed from sites down the continental slope in the Bay of Biscay. Within the internal gravity wave band kinetic energy spectra were dominated near localized frequencies associated with the local inertial frequency and the semidiurnal tidal frequency, and their non-linear interaction frequencies. The major conclusion was that the relative bandwidth near all these frequencies was constant (~ 0.09), so that the number of waves within a group was independent of frequency. This confirmed the non-linear forcing of super-tidal internal waves associated with inertial–tidal interactions. It is suggested that the fundamental (inertial, tidal) frequencies had the same interaction with stratification and background shear, so that the mean ocean (internal wave) response was

similar despite their completely different mechanical forcing.

Acknowledgements

I enjoyed the assistance of the crew of the R/V *Pelagia* in the deployment and recovery of all moorings. I thank the anonymous referees for their useful comments and Allison Lee for editorial advice. I am indebted to Prof. Gerold Siedler (IfM Kiel) for the use of his Canary Basin data. Margriet Hiehle produced Fig. 1. I thank Hendrik van Aken for the use of current meter data from his project 'TripleB' in the Bay of Biscay, which has been supported by a grant from the Netherlands organization for the advancement of scientific research, NWO. This is NIOZ contribution 3607.

References

Alford, M.H., 2001. Fine-structure contamination: observations and a model of a simple two-wave case. Journal of Physical Oceanography 31, 2645–2649.

Benjamin, T.B., Feir, J.E., 1967. The disintegration of wave trains on deep water, part 1. Theory. Journal of Fluid Mechanics 27, 417–430.

Brekhovskikh, L.M., Konjaev, K.V., Sabinin, K.D., Serikov, A.N., 1975. Short-period internal waves in the sea. Journal of Geophysical Research 80, 856–864.

Briscoe, M.G., 1999. Short-term directional variability of the continuum range in the deep-ocean internal wave field. In: Müller, P., Henderson, D. (Eds.), Dynamics of Oceanic Internal Gravity Waves, II. Proceedings 'Aha Huliko'a Hawaiian Winter Workshop. SOEST, Hawaii, pp. 169–172.

D'Asaro, E.A., Perkins, H., 1984. A near-inertial internal wave spectrum for the Sargasso Sea in late summer. Journal of Physical Oceanography 14, 489–505.

Dronkers, J.J., 1964. Tidal Computations in Rivers and Coastal Waters. North-Holland Publishing Company, Amsterdam, 518pp.

Ekman, V.W., 1931. On internal waves. Rapports et Procès-Verbaux des Réunions du Conseil Permanent International pour l'Exploration de la Mer 76, 5–34.

Fu, L.-L., 1981. Observations and models of inertial waves in the deep ocean. Reviews of Geophysics and Space Physics 19, 141–170.

Garrett, C., 2001. What is the "near-inertial" band and why is it different from the rest of the internal wave spectrum? Journal of Physical Oceanography 31, 962–971.

Garrett, C.J.R., Munk, W.H., 1972. Space-time scales of internal waves. Geophysical Fluid Dynamics 3, 225–264.

Gerkema, T., 2001. Internal and interfacial tides: beam scattering and local generation of solitary waves. Journal of Marine Research 59, 227–255.

Gerkema, T., 2002. Application of an internal tide generation model to baroclinic spring–neap cycles. Journal of Geophysical Research 107(C9), 3124, doi: 10.1029/2001JC001177.

Gill, A.E., 1982. Atmosphere-Ocean Dynamics. Academic Press Inc., Orlando, Fl, 662 pp.

Gonella, J., 1972. A rotary-component method for analysing meteorological and oceanographic vector time series. Deep-Sea Research 19, 833–846.

Hasselmann, K., Barnett, T.P., Bouws, E., Carlson, H., Cartwright, D.E., Enke, K., Ewing, J.A., Gienapp, H., Hasselmann, D.E., Kruseman, P., Meerburg, A., Müller, P., Olbers, D.J., Richter, K., Sell, W., Walden, H., 1973. Measurements of wind-wave growth and swell decay during the Joint North Sea Wave Project (JONSWAP). Deutsches. Hydrographisches Zeitschrift Supplement A 8 (12), 1–95.

Huthnance, J.M., Baines, P.G., 1982. Tidal currents in the northwest African upwelling region. Deep-Sea Research 29, 285–306.

Jenkins, G.M., Watts, D.G., 1968. Spectral Analysis and its Applications. Holden-Day, San Fransisco, CA, 525pp.

Kundu, P.K., 1993. On internal waves generated by travelling wind. Journal of Fluid Mechanics 254, 529–559.

Kunze, E., 1985. Near-inertial wave propagation in geostrophic shear. Journal of Physical Oceanography 15, 544–565.

Levine, M.D., 1991. Observing oceanic internal waves: what have we learned? What can we learn? In: Müller, P., Henderson, D. (Eds.), Dynamics of Oceanic Internal Gravity Waves. Proceedings 'Aha Huliko'a Hawaiian Winter Workshop. SOEST, Hawaii, pp. 467–479.

Longuet-Higgins, M.S., 1984. Statistical properties of wave groups in a random sea state. Philosophical Transactions of the Royal Society of London A 312, 219–250.

Magaard, L., McKee, W.D., 1973. Semi-diurnal tidal currents at 'site D'. Deep-Sea Research 20, 997–1009.

Marmorino, G.O., 1987. Observations of small-scale mixing processes in the seasonal thermocline. Part II: wave breaking. Journal of Physical Oceanography 17, 1348–1355.

Marmorino, G.O., Rosenblum, L.J., Trump, C.L., 1987. Fine-scale temperature variability: the influence of near-inertial waves. Journal of Geophysical Research 92, 13,049–13,062.

Mihaly, S.F., Thomson, R.E., Rabinovich, A.B., 1998. Evidence for non-linear interaction between internal waves of inertial and semidiurnal frequency. Geophysical Research Letters 25, 1205–1208.

Mooers, C.N.K., 1975. Several effects of a baroclinic current on the cross-stream propagation of inertial-internal waves. Geophysical Fluid Dynamics 6, 245–275.

Munk, W.H., 1980. Internal wave spectra at the buoyant and inertial frequencies. Journal of Physical Oceanography 10, 1718–1728.

Munk, W., Phillips, N., 1968. Coherence and band structure of inertial motion in the sea. Reviews of Geophysics 6, 447–472.

Ozmidov, R.V., 1965. Energy distribution between oceanic motions of different scales. Izvestia Atmospheric Ocean Physics 1, 257–261.

Parks, T.W., Burrus, C.S., 1987. Digital Filter Design. Wiley, New York, 342pp.

Pingree, R.D., Maddock, L., 1978. The M_4 tide in the English Channel derived from a non-linear numerical model of the M_2 tide. Deep-Sea Research 26, 53–68.

Pingree, R.D., New, A.L., 1991. Abyssal penetration and bottom reflection of internal tidal energy in the Bay of Biscay. Journal of Physical Oceanography 21, 28–39.

Pollard, R.T., Millard, R.C., 1970. Comparison between observed and simulated wind-generated inertial oscillations. Deep-Sea Research 17, 813–821.

Pugh, D.T., 1987. Tides, Surges and Mean Sea-level. Wiley, Chichester, 472pp.

Rossiter, J.R., Lennon, G.W., 1968. An intensive analysis of shallow water tides. Geophysical Journal of the Royal astronomical Society 16, 275–293.

Schott, F., 1977. On the energetics of baroclinic tides in the North Atlantic. Annales de Geophysique 33, 41–62.

Siedler, G., Paul, U., 1991. Barotropic and baroclinic tidal currents in the eastern basins of the North Atlantic. Journal of Geophysical Research 96, 22,259–22,271.

Stewartson, K., Walton, I.C., 1976. On inertial oscillations in the ocean. Tellus 28, 71–73.

St. Laurent, L., Garrett, C., 2002. The role of internal tides in mixing the deep ocean. Journal of Physical Oceanography 32, 2882–2899.

Thorpe, S.A., 1999. On internal wave groups. Journal of Physical Oceanography 29, 1085–1095.

van Haren, H., 2003. On the polarization of oscillatory currents in the Bay of Biscay. Journal of Geophysical Research 108(C9), 3290, doi:10.1029/2002JC001736.

van Haren, H., 2004. Incoherent internal tidal currents in the deep ocean. Ocean Dynamics 54, 66–76.

van Haren, J.J.M., Maas, L.R.M., 1987. Temperature and current fluctuations due to tidal advection of a front. Netherlands Journal of Sea Research 21, 79–94.

van Haren, H., Maas, L., Zimmerman, J.T.F., Ridderinkhof, H., Malschaert, H., 1999. Strong inertial currents and marginal internal wave stability in the central North Sea. Geophysical Research Letters 26, 2993–2996.

van Haren, H., Maas, L., van Aken, H., 2002. On the nature of internal wave spectra near a continental slope. Geophysical Research Letters 29(12), doi:10.1029/2001GL014341. (Corrigendum: 2003, 30(7), doi:10.1029/2003GL016952).

Xing, J., Davies, A.M., 2002. Processes influencing the nonlinear interaction between inertial oscillations, near inertial internal waves and internal tides. Geophysical Research Letters 29(5), 1067, doi:10.1029/2001GL014199.

Webster, F., 1968. Observations of inertial-period motions in the deep sea. Reviews of Geophysics 6, 473–490.

Wunsch, C., 1975. Internal tides in the ocean. Reviews of Geophysics and Space Physics 13, 167–182.